

# **L shell x-ray production in high-Z elements using 4-6 MeV/u fluorine ions**

Sunil Kumar<sup>1,2</sup>, Udai Singh<sup>2</sup>, M. Oswal<sup>3</sup>, G. Singh<sup>1</sup>, N. Singh<sup>1</sup>, D. Mehta<sup>1</sup>, G. Lapicki<sup>4</sup> and T. Nandi<sup>5\*</sup>

<sup>1</sup>*Department of Physics, Panjab University, Chandigarh 160014, India.*

<sup>2</sup>*Department of Applied Sciences, Chitkara University, Himachal Pradesh 174103, India.*

<sup>3</sup>*Department of Physics, Dev Samaj College Sec 45-B Chandigarh 160047, India*

<sup>4</sup>*Department of Physics, East Carolina University, Greenville, North Carolina 27858, USA.*

<sup>5</sup>*Inter-University Accelerator Centre, New Delhi 110067, India.*

## **Abstract**

L shell line and total x-ray production cross sections in  $^{78}\text{Pt}$ ,  $^{79}\text{Au}$ ,  $^{82}\text{Pb}$ ,  $^{83}\text{Bi}$ ,  $^{90}\text{Th}$ , and  $^{92}\text{U}$  targets ionized by 4-6 MeV/u fluorine ions were measured. These cross sections are compared with available theories for L shell ionization using single- and multiple-hole fluorescence and the Coster-Kronig yields. The ECPSSR and the ECUSAR theories exhibit good agreement with the measured data, whereas, the FBA theory overestimates them by a factor of two. Although for the F ion charge states  $q = 6-8$  the multiple-hole atomic parameters do not significantly differ from the single-hole values, after an account for the multiple-holes, our data are better in agreement with the ECUSAR than the ECPSSR theory.

**Keywords:** L-shell x-rays, heavy ions, ionization, multiple ionization.

PACS number(s): 34.50.Fa, 34.80.Dp, 31.15.xp, 32.30.Rj

*\*Corresponding Author.*

**Email:** [nanditapan@gmail.com](mailto:nanditapan@gmail.com)

## 1. INTRODUCTION

The measurement of emitted x-rays from targets has resulted in major advances in radiation[1], plasma [2], atomic and nuclear physics [3], and in particle induced x-ray emission (PIXE) technique [4,5]. While PIXE originated and continues using light ions such as protons or alphas [6–16], there is an increasing interest to use heavy ions for PIXE analysis due to higher cross sections and thereby better sensitivity [17]. While discrepancies between theories and experiment were attributed to multiple ionization even with protons[18], multiple-ionization effect has been known for decades in L-shell ionization by heavier ions [19–34]. However this effect is still rarely addressed for the x-ray emission elemental analysis in the aftermath of ionization by such ions.

The sum of electron capture (EC) from a projectile with the atomic number  $Z_P$  and direct ionization (DI) of a target with the atomic number  $Z_T$  results in ionization of the target atom's inner shells. In asymmetric collisions, i.e.,  $Z_P/Z_T \ll 1$ , the DI is dominant, whereas, for symmetric collisions, i.e., with  $Z_P/Z_T$  approaching 1, the EC process becomes increasingly important. As presented in Section 2, the L shell x-ray production cross sections have been measured in high  $Z_T$ -targets ionized by the 76–114 MeV  $^{19}\text{F}$  ions. With  $Z_P = 9$ ,  $0.010 \leq Z_P/Z_T \leq 0.012$  and the ratio of the projectile velocity  $v_p = 6.351 [E_P(\text{MeV})/A_P(\text{u})]^{1/2}$  (a.u) to the orbital velocity of the L-shell electrons  $v_T = (Z_T - 4.15)/2$  less than 1 i.e.,  $0.029 \leq v_p/v_T \leq 0.042$ , the present data are in the asymmetric and slow collision regime.

While expanding on the existing data base with ionization by heavy ions as desired for PIXE analysis, the collision regime of the present data allows for a meaningful comparison with existing ionization theories as discussed in Section 3. Section 4 addresses effects of the single- and multiple-hole atomic parameters required for conversion of ionization to x-ray production cross sections, and Section 5 summarizes our findings.

## 2. EXPERIMENTAL DETAILS AND DATA ANALYSIS

The L shell x-ray production cross sections in the elements with  $78 \leq Z_T \leq 92$  elements using the  $^{19}\text{F}$  ions (charge states  $q = 6^+, 7^+, 8^+$ ) in the 76 – 114 MeV energy range had been measured. Heavy ions of  $\text{F}^{6+}$  (76 and 84 MeV),  $\text{F}^{7+}$  (90 MeV) and  $\text{F}^{8+}$  (98, 106 and 114 MeV) were obtained from the 15 UD Pelletron accelerator at Inter-University Accelerator Centre,

New Delhi. Two silicon surface barrier detectors at  $\pm 7.5^\circ$  to the beam direction were used to monitor the projectile ions. The chamber was evacuated to about  $10^{-6}$  Torr and equipped with a 5 mm diameter collimator and 6  $\mu\text{m}$  Mylar window in front of the Si(Li) detector. In the energy range of the measured L x-ray spectra, the energy resolution of the detector was  $\sim 200$  eV for the Mn  $K\alpha$  x rays. A Si(Li) solid state detector (thickness = 5 mm, diameter = 10 mm, 25  $\mu\text{m}$  Be window from ORTEC, Oak Ridge, Tennessee, USA) was placed in the horizontal ion beam plane configuration outside the vacuum chamber at an angle of  $125^\circ$  to the beam direction and a distance of 170 mm from the target. The targets were mounted on a steel ladder at a  $90^\circ$  angle to the beam direction. The ladder could accommodate up to 24 targets (8 rows and 3 columns) each of 11.7 mm diameter and the desired target was brought along the beam direction by the horizontal and the vertical movement of the target ladder using the stepper motor arrangement. The spot size of the ion beam at the target was  $\sim 2$  mm diameter. The spectra were taken at different positions of each target by tiny steering the beam. The thickness and the uniformity of these targets were measured by the energy loss method using alpha particles from a radioactive decay of  $^{241}\text{Am}$ . Targets of  $^{78}\text{Pt}$ ,  $^{79}\text{Au}$ ,  $^{82}\text{Pb}$ , and  $^{83}\text{Bi}$  (thickness  $\sim 120 \mu\text{g}/\text{cm}^2$ ) were prepared on the  $20 \mu\text{g}/\text{cm}^2$  carbon backing using the vacuum deposition technique [35]. Thinner and spectroscopically pure (99.999 % pure) targets of  $\text{ThF}_4$  ( $48.7 \mu\text{g}/\text{cm}^2$ ) and  $\text{UF}_4$  ( $48.6 \mu\text{g}/\text{cm}^2$ ) on Mylar backing (thickness = 3  $\mu\text{m}$ ) procured from Micromatter, Deer Harbor, Washington, USA were also used in the present work. The target uniformity was verified to be better than 5%. The beam current was kept below 1nA to avoid the pile up effects and the damage to the target. The spectra were collected for 30 minutes to 1 hour so as to get good statistical accuracy.

Figure 1 shows typical L x-ray spectra from the targets of  $^{78}\text{Pt}$ ,  $^{79}\text{Au}$ ,  $^{82}\text{Pb}$ ,  $^{83}\text{Bi}$ ,  $^{90}\text{Th}$ , and  $^{92}\text{U}$  elements ionized by the 98 MeV  $^{19}\text{F}$  ions. These spectra result from ionization of  $L_i$  ( $i = 1-3$ ) subshells, with which x-ray line peaks correlate viz.,  $L\ell$ ,  $L\alpha_{1,2}$ , and  $L\beta_{2,15,6,7}$  from the  $L_3$  subshell, the  $L\eta$ ,  $L\beta_1$ , and  $L\gamma_{1,5}$  from the  $L_2$  subshell, and the  $L\beta_{3,4}$  and  $L\gamma_{2,3,4}$  from the  $L_1$  subshell. Figure 2 displays L x-ray spectra of  $^{92}\text{U}$  target bombarded by the  $^{19}\text{F}$  ion beam at different energies. The differential L x-ray production cross sections for the major peaks were evaluated with

$$\frac{d\sigma_i^x}{d\Omega} = \frac{N_x A}{N_A N_p t \epsilon \beta} \quad (1)$$

where  $N_x$  is the net x-ray counts per second under the L x-ray peak,  $A$  is atomic mass (in grams),  $N_A$  is the Avogadro's number, and  $N_p$  is the number of incident ions collected in the Faraday cup. The ion beam changes its charge state during its passage through the target. The mean distribution in charge state of ion beam after passing through the target and its backing is calculated using the computer code ETACHA [36]. This code accounts for electron loss, capture, and excitation from and to all the subshells based on an independent electron model. The measured charge in the Faraday cup using a current integrator has been corrected for the change in the charge state and used for  $N_p$  with the incident charge state in Equation (1). Also in this equation,  $t$  is the target thickness in  $\mu\text{g}/\text{cm}^2$ ,  $\varepsilon$  is the absolute detection efficiency (included all absorbing components of the set-up), and  $\beta \equiv [1 - \exp(-\mu t)]/\mu t$  is the correction factor for the absorption of the emitted L x-rays in the present target, where  $\mu$  in  $\text{cm}^2/\mu\text{g}$  is the attenuation coefficient [37]. The  $\beta$  is  $\geq 0.99$  for the target thickness used in the present measurements. The energy loss calculation using the SRIM code [38] for the incident beam within the target suggests negligibly small energy loss for the target thickness and the beam energies used in the present work. For example, 76 and 114 MeV fluorine ion lose 267 and 223 keV in Pt, and 104 and 87 keV in U target, respectively. The peak areas,  $N_x$ , are evaluated using the computer program CANDLER [39]. This software is an improved version of the Levenburg-Marquardt [40] non-linear minimization algorithms for the peak fitting. The FWHM for the intrinsic Lorentzian broadening associated with the L x-ray lines is  $< 12$  eV [41]. The energy calibration of the detector is performed before and after the in-beam measurements. Relative efficiency of the x-ray detector in the energy region of interest is deduced by measuring the fluorescence K x-ray yields from various elemental targets excited by the 59.54 keV photons from a point 100 mCi  $^{241}\text{Am}$  source, which was mounted in the chamber instead of the ion beam. The Cu-Al attenuator of suitable thickness is used with the source to remove the low energy  $^{93}\text{Nb}$  L x-rays and 26 keV  $\gamma$ -ray emitted from the source. Thick targets of  $^{26}\text{Fe}$ ,  $^{28}\text{Ni}$ ,  $^{29}\text{Cu}$ ,  $^{30}\text{Zn}$ ,  $^{33}\text{As}$ ,  $^{34}\text{Se}$ ,  $^{39}\text{Y}$ ,  $^{40}\text{Zr}$ ,  $^{41}\text{Nb}$ ,  $^{42}\text{Mo}$ ,  $^{46}\text{Pd}$ ,  $^{47}\text{Ag}$ ,  $^{48}\text{Cd}$ ,  $^{49}\text{In}$ , and  $^{50}\text{Sn}$  elements were excited by the 59.54 keV photons. The efficiency of the detector is calculated from

$$I_0 \Omega \varepsilon_{\text{KX}} = \frac{4\pi N_{\text{KX}}}{\sigma_{\text{KX}} t \beta_{\text{KX}}} \quad (2)$$

where  $I_0$  is the intensity of the incident photons to be collected into the solid angle  $\Omega$  and  $\varepsilon_{\text{KX}}$  is the absorption of the x-rays in air and Mylar window.  $N_{\text{KX}}$  is the measured count rate under the K x-ray peak, while  $\sigma_{\text{KX}}$  is calculated as product of the K shell photoionization cross section

[42] the fluorescence yield [43,44], and the fractional emission rates [45] for the  $K\alpha$  and  $K\beta$  x-rays. As in Eq.(1),  $t$  is the thickness of target element and  $\beta_{KX}$  is the absorption correction factor that now depends both on the incident  $\theta_i$  and emitted angles  $\theta_e$  with respect to the normal to the target. This self-absorption correction factor, accounting for the attenuation of the incident and the emitted K x-rays of the target element, is given by

$$\beta_{KX} = \frac{1 - \exp[-(\mu_i/\cos\theta_i + \mu_e/\cos\theta_e)t]}{(\mu_i/\cos\theta_i + \mu_e/\cos\theta_e)t} \quad (3)$$

where,  $\mu_i$  and  $\mu_e$  are the mass-attenuation coefficients for the incident and the emitted x-rays in the target calculated using XCOM [37]. A semi-empirically fitted relative efficiency curve is generated by taking into account the absorption of the various K x-rays of the target elements. Figure 3 shows the absolute efficiency  $\mathcal{E}$  of the Si(Li) detector obtained using the calibrated radioactive sources of  $^{137}\text{Cs}$  and  $^{155}\text{Eu}$ . The relative efficiency curve obtained by measuring the K x-ray yields is normalized with respect to the absolute source strength to obtain an absolute efficiency curve.

Although the L<sub>I</sub> line that is weakest in L x-ray spectra is not perfectly isotropic [46–48] differential x-ray production cross sections have been measured at an emission angle  $\Psi = 125^\circ$  where the second-order Legendre polynomial term,  $P_2(\cos\Psi) \approx 0$ . Thus integrated x-ray production cross sections were deduced by multiplying the differential cross sections of Eq.(1) by a factor of  $4\pi$ .

The percentage error in the measured x-ray production cross sections is about 10-15%. This error is attributed to the uncertainties in different parameters used in the analysis, namely, the photopeak area evaluation ( $\sim 5\%$  for the L<sub>I</sub> x-ray peak and 3% for the other peaks), ion beam current ( $\sim 7\%$ ), target thickness ( $\sim 3\%$ ). The error in the absolute efficiency values,  $\mathcal{E}$ , is 5-8% in the energy region of interest. The measured cross sections taken for an element from different locations on the same target are found to agree within the experimental error and their weighted average is given in Table 1.

### 3. IONIZATION THEORIES

Direct ionization (DI) of inner shells can be calculated with the plane wave Born approximation (PWBA) [49–51], binary encounter approximation (BEA) [7,52] and semi-classical approximation (SCA) [53] while the Oppenheimer-Brinkman-Kramers formulation of Nikolaev (OBKN) [54] may be used to evaluate electron capture (EC). The sum of the PWBA and OBKN constitute the first Born approximation (FBA) for inner-shell ionization [49–51,54] calculations. An approach that goes beyond the FBA is the ECPSSR theory that accounts the energy-loss (E) and Coulomb-deflection (C) of the projectile and perturbed-stationary state (PSS) and relativistic (R) nature of the target's inner shells [55]. PSS formulas of the ECPSSR theory were further modified for united and separated atom (USA) treatments of the electron wave function to generate the ECUSAR theory [56].

The theoretical x-ray production cross sections  $\sigma_{Lp}^x$  ( $p = 1, \alpha, \beta, \gamma$ ) for the most commonly resolved  $L_1$ ,  $L\alpha$ ,  $L\beta$ , and  $L\gamma$  lines are related to the  $\sigma_{L_i}$  ( $i = 1-3$ ) that are the ionization cross sections for the  $L_1$ ,  $L_2$ , and  $L_3$  as

$$\sigma_{L_1} = [\sigma_{L_1}(f_{12}f_{23} + f_{13}) + \sigma_{L_2}f_{23} + \sigma_{L_3}] \omega_3 F_{3l} \quad (4a)$$

$$\sigma_{L\alpha}^x = [\sigma_{L_1}(f_{12}f_{23} + f_{13}) + \sigma_{L_2}f_{23} + \sigma_{L_3}] \omega_3 F_{3\alpha} \quad (4b)$$

$$\sigma_{L\beta}^x = \sigma_{L_1} [\omega_1 F_{1\beta} + f_{12} \omega_2 F_{2\beta} + (f_{12}f_{23} + f_{13}) \omega_3 F_{3\beta}] + \sigma_{L_2} (\omega_2 F_{2\beta} + f_{23} \omega_3 F_{3\beta}) + \sigma_{L_3} \omega_3 F_{3\beta} \quad (4c)$$

$$\sigma_{L\gamma}^x = \sigma_{L_1} (\omega_1 F_{1\gamma} + f_{12} \omega_2 F_{2\gamma}) + \sigma_{L_2} \omega_2 F_{2\gamma} \quad (4d)$$

The measured L line x-ray production cross sections and the calculated ones using the  $L_i$  subshell ionization cross sections from different theories including the correction for multiple ionization (MI) effects, *viz.*, FBA-MI [49–51,54], ECPSSR-MI [55], and ECUSAR-MI [56] are given in Table 1. The theoretical cross sections have been calculated using the  $L_i$  subshell ionization cross sections corresponding to the incident ion charge state. A representative case of  $L_i$  subshell ionization in gold bombarded by different charge states of  $^{19}\text{F}$  projectile ions based on the FBA [49–51,54] and ECUSAR [56] is shown in the Figure 4.  $F_{ip}$  ( $i= 1-3, p = 1, \alpha, \beta, \gamma$ ) are the radiative fractional emission rates. The L x-ray emission rates based on DHS calculation [57] and the interpolated values by Campbell and Wang [45] have been used in the present measurements. For the two datasets of  $F_{3\beta}$ ,  $F_{1\gamma}$ , and  $F_{2\gamma}$  values, the difference is 5-8% over the atomic range  $Z_T = 50-92$ , whereas, other values of the emission rates differ from each other by

less than 4%. The parameters  $\omega_i$  ( $i = 1-3$ ) are the fluorescence yields of the  $L_i$  subshells and  $f_{ij}$  ( $i < j$ ) are the CK yields for the transition between  $L_i$  and  $L_j$  subshells. The single-hole fluorescence  $\omega_i^0$  and CK yields  $f_{ij}^0$  can be obtained from Krause [58] and Chen *et al.* [59]. As given in Table 2, the datasets of  $\omega_i^0$  and  $f_{ij}^0$  significantly differ from each other. For the present elements under consideration, the  $f_{13}^0$  (Rec.) values are on the average about 15% lower than the  $f_{13}^0$  (DHS) values and  $\sim 9\%$  higher than the  $f_{13}^0$  (Krause) values. The  $f_{12}^0$  (Rec.) values differ  $\sim 15\%$  in average higher than the  $f_{12}^0$  (DHS) values and are about half the  $f_{12}^0$  (Krause) values. The  $f_{23}^0$  (Rec.) values from different sets do not differ significantly. The  $\omega_2^0$  (Rec.) and  $\omega_3^0$  (Rec.) values agree with the DHS values and are higher from Krause's values below 10% for the present elements. The  $\omega_1^0$  (Rec.) values differ from  $\omega_1^0$  (Krause) values by 0-14% and from  $\omega_1^0$  (DHS) by 13-52%. The use of different sets of atomic parameters can change x-ray production cross section by  $\sim 30\%$ . Recent values of  $\omega_i^0$  and  $f_{ij}^0$  compiled by Campbell [43,44] for the elements with  $25 \leq Z \leq 96$  have been used in the present work for singly-ionized atoms.

#### 4. EFFECT OF SINGLE- AND MULTIPLE-HOLE ATOMIC PARAMETERS ON THE CONVERSION OF IONIZATION TO X-RAY PRODUCTION CROSS SECTIONS

Multiple vacancies in the target atom change the atomic parameters by increasing fluorescence yields and decreasing CK yields which in turn enhances x-ray production cross sections. In the present work, single-hole fluorescence  $\omega_i^0$  and CK yields  $f_{ij}^0$  [43], were corrected for multiple ionization using a model prescribed by Lapicki *et al.* [60]. Each electron in a manifold of the outer subshells is ionized with a probability  $P$  which is calculated from Equation (A3) of [60] and replacing the projectile atomic number  $Z_P$  by its charge state  $q$  [61],

$$P = \frac{q^2}{2\beta v_P^2} \left( 1 - \frac{\beta}{4v_P^2} \right) \quad (5)$$

With  $\beta = 0.9$ . For charge state  $q$ , we take the incident charge state of the projectile. The  $\omega_i^0$  values corrected for simultaneous ionization in outer subshells are given by

$$\omega_i = \omega_i^0 [1 - P(1 - \omega_i^0)]^{-1} \quad (6)$$

While the  $f_{ij}$  values for multiple ionization are given by

$$f_{ij} = f_{ij}^0 (1 - P)^2. \quad (7)$$

Note that the fractional rates  $F_{ip}$  remain unchanged because both partial and total non-radiative widths are narrowed by identical factors. With Eq. (6) and Eq. (7), the single-hole fluorescence and CK yields change at different ion beam energies and charge states. Fluorescence and CK yields for singly- and multiply-ionized  $^{78}\text{Pt}$  and  $^{92}\text{U}$  elements are given in Table 3. It is clear from this table that in the extreme the  $L_i$  subshell fluorescence yields are enhanced by  $\sim 15\%$  and CK yields are reduced up to  $\sim 27\%$  from single-hole to multiple-hole atom in  $^{78}\text{Pt}$ . These values differ by 2-3% over the range of the ion beam energies and the projectile charge states used in the present experiment.

L-shell line and total x-ray production cross sections, at corresponding energies and incident charge state of the fluorine ions, are listed in Table 1 and shown in Figures 5-7. Although the connection between observed L x-ray lines and calculated  $L_i$  subshell ionization cross sections depends on a combination of intra-shell coupling and inner shell multiple ionization effects [62,63], the data for ionization of comparably heavy targets as ours but by significantly slower 4-8 MeV carbon ions [64] show that multiple-ionization is more effective. While both effects subside in the 4-6 MeV/amu range of the present experiment, the effect of the intra-shell coupling is overshadowed by multiple ionization [64]. Thus in Table 1, ignoring the negligible effect the intra-shell coupling, all measured cross sections are compared to the predictions of the FBA [49–51,54], ECPSSR [55], and ECUSAR [56] ionization theories converted to the x-ray production cross sections using multiple-hole atomic parameters calculated with Eqs.(5)-(7). Within experimental error, the ratios of our data to ECPSSR [55] and ECUSAR [56] are practically the same at  $q = 6^+$  and  $q = 7^+$ ; at  $q = 8^+$ , ECUSAR [56] is distinctly better than ECPSSR[55]. After averaging over energies and charge states, for each element Table 4 shows the standard deviations of the so calculated x-ray production cross sections from our measurements. For comparison this table also shows the standard deviations when the ionization theories are converted with single-hole atomic parameters that are listed in Table 3. Theories converted with multiply-ionized atomic parameters are clearly in better agreement with our data.

## 5. CONCLUSIONS

In the present work, the L x-ray production cross sections of  $^{78}\text{Pt}$ ,  $^{79}\text{Au}$ ,  $^{82}\text{Pb}$ ,  $^{83}\text{Bi}$ ,  $^{90}\text{Th}$ , and  $^{92}\text{U}$  elements for the incident  $^{19}\text{F}$  ions of charge states  $6^+$ ,  $7^+$  and  $8^+$  have been measured. These data were compared with the theoretical L x-ray production cross section calculated from the  $L_i$  ( $i = 1-3$ ) subshell ionization cross sections using FBA, ECPSSR and ECUSAR and recently



recommended set of the  $L_i$  ( $i = 1-3$ ) subshell fluorescence and CK yields with and without modifications for the multiple vacancies in the outer shells. While the measured values are about two times lower than those calculated using the FBA, exhibit agreement with those based on the ECPSSR and ECUSAR calculations. This is particularly so when the fluorescence yields are corrected for the outer-shell multiple ionization. Although the ionization cross sections for the  $^{19}\text{F}$  ions with the  $6^+$ ,  $7^+$ , and  $8^+$  charge states over the ion beam energies used in the present work are almost independent of the charge state, the multiple ionization effect is essentially equal in the ECPSSR-MI and ECUSAR-MI calculations for  $q = 6^+$  and  $7^+$ . At  $q = 8^+$ , the ECUSAR-MI agrees better with the data than the ECPSSR-MI theory.

Singh et al.[28] reported L-x ray production cross sections in gold and bismuth with fluorine ions at 83 and 98 MeV of essentially the same charge state as the present data. While for  $^{79}\text{Au}$  their total cross sections fluctuate from as much as 7% above ours at 84 MeV to as much as 27% below ours at 98 MeV, for  $^{83}\text{Bi}$  their measurements are below ours by about 22% at 84 MeV and almost 43% below at 98 MeV. Even with a conservative estimate of 20% for experimental errors, the discrepancies between the Singh et al.[28] and our measurements are difficult to explain, and suggest that - aside from its inherent interest for comparison with theories and PIXE applications - it would be worth for other experimentalists to revisit this collision regime.

### **Acknowledgements**

Financial support from the Science and Engineering Research Board (SERB), New Delhi to Dr. Sunil Kumar in terms of Young Scientist scheme and grant from IUAC, New Delhi in terms of UF-UP-43302 project is highly acknowledged. Author also acknowledges the work of Pelletron staff for smooth conduct of experiment.

## Figure Captions

**Fig.1** L x-ray spectra from  $^{78}\text{Pt}$ ,  $^{79}\text{Au}$ ,  $^{82}\text{Pb}$ ,  $^{83}\text{Bi}$ ,  $\text{ThF}_4$ ,  $\text{UF}_4$  bombarded with the 98 MeV  $^{19}\text{F}$  ions.

**Fig.2** L x-ray spectra from  $^{92}\text{U}$  ( $48.6 \mu\text{g}/\text{cm}^2$   $\text{UF}_4$  target) bombarded with 76, 84, 90, 98, 106, and 114 MeV  $^{19}\text{F}$  ions,

**Fig.3** Efficiency curve obtained by measuring the K x-rays fluorescence yields from targets excited by the 59.54 keV  $\gamma$ -ray photons. Measured values were normalized to absolute efficiency obtained using the calibrated  $^{137}\text{Cs}$  and  $^{155}\text{Eu}$  radioactive sources.

**Fig.4**  $L_i$  subshell ionization in gold bombarded by  $^{19}\text{F}$  ions based on the FBA [49–51,54] and ECUSAR [56].

**Fig.5**  $L\text{I}$ ,  $L\gamma$ ,  $L\beta$ ,  $L\alpha$  and total L x-ray production in  $^{78}\text{Pt}$  and  $^{79}\text{Au}$  targets bombarded by  $^{19}\text{F}$  ions according to FBA-MI, ECUSAR-MI, and present measurements.

**Fig.6**  $L\text{I}$ ,  $L\gamma$ ,  $L\beta$ ,  $L\alpha$  and total L x-ray production in  $^{82}\text{Pb}$  and  $^{83}\text{Bi}$  targets bombarded by  $^{19}\text{F}$  ions according to FBA-MI, ECUSAR-MI, and present measurements.

**Fig.7**  $L\text{I}$ ,  $L\gamma$ ,  $L\beta$ ,  $L\alpha$  and total L x-ray production in  $^{90}\text{Th}$  and  $^{92}\text{U}$  targets bombarded by  $^{19}\text{F}$  ions according to FBA-MI, ECUSAR-MI, and present measurements.

## References

- [1] Satoh T 2015 Development of particle induced X-ray emission-computed tomography in Takasaki Advanced Radiation Research Institute, Japan Atomic Energy Agency *Int. J. PIXE* **25** 147
- [2] Sharma P and Nandi T 2016 Experimental evidence of beam-foil plasma creation during ion-solid interaction *Phys. Plasmas* **23** 83102
- [3] Dyson N A 1990 *X-rays in atomic and nuclear physics* (Cambridge University Press)
- [4] Antoszewska-Moneta M, Brzozowski R and Moneta M 2015 Modification of thin films induced by slow heavy ions analysed with PIXE and SRIM *Eur. Phys. J. D* **69** 77
- [5] Gillespie A W, Phillips C L, Dynes J J, Chevrier D, Regier T Z and Peak D 2015 Advances in Using Soft X-Ray Spectroscopy for Measurement of Soil Biogeochemical Processes *Adv. Agron.* **133** 1
- [6] Johansson T B, Akselsson R and Johansson S A E 1970 X-ray analysis: Elemental trace analysis at the 10-12 g level *Nucl. Inst. Meths. B* **84** 141
- [7] Garcia J D 1970 Inner-Shell Ionizations by Proton Impact *Phys. Rev. A* **1** 280
- [8] Richard P 1975 *Ion-Atom Collisions, in Atomic Inner-Shell Processes* ed B Crasemann (New York: Academic Press) Vol.I p.79
- [9] Joseph D, Nageshwara Rao S V S and Kailas S 2013 Measurement of L X-Ray Production Cross-Sections of Au , Ho , Bi and K-X-Ray Cross Sections of Nb , Sn , Sb by Using Protons of Energy 4 MeV *Mapana J. Sci.* **12** 1
- [10] Zhou X, Zhao Y, Cheng R, Wang Y, Lei Y, Wang X and Sun Y 2013 K and L-shell X-ray production cross sections for 50–250 keV proton impact on elements with Z=26–30 *Nucl. Inst. Meths. B* **299** 61
- [11] Miranda J, Murillo G, Méndez B, López-Monroy J, Aspiazú J, Villaseñor P, Pineda J C and Reyes-Herrera J 2013 Measurement of L X-ray production cross sections by impact of proton beams on Hf, Ir, and Tl *Nucl. Inst. Meths. B* **316** 113
- [12] Bertol A P L, Trincavelli J, Hinrichs R and Vasconcellos M A Z 2014 L-shell X-ray production cross sections induced by protons and alpha-particles in the 0.7-2.0 MeV/amu range for Ru and Ag *Nucl. Instr. Meth. B* **318** 19
- [13] Batyrbekov E, Gorlachev I, Ivanov I and Platov A 2014 K-, L- and M-shell x-ray production cross sections by 1–1.3MeV protons *Nucl. Instr. Meth. B* **325** 84
- [14] Miranda J and Lapicki G 2014 Experimental cross sections for L-shell x-ray production and ionization by protons *At. Data Nucl. Data Tables* **100** 651

- [15] Mohan H, Jain A K, Kaur M, Singh P S and Sharma S 2014 Cross section for induced L X-ray emission by protons of energy  $< 400\text{keV}$  *Nucl. Instr. Meth. B* **332** 103
- [16] Bertol A P L, Hinrichs R and Vasconcellos M A Z 2015 Proton induced L1, L2, L3-sub-shell X-ray production cross sections of Hf and Au *Nucl. Instr. Meth. B* **363** 28
- [17] Siegele R, Cohen D D and Dytlewski N 1999 The ANSTO high energy heavy ion microprobe *Nucl. Instr. Meths. B* **158** 31
- [18] Naga Raju G J, Ramana Murty G A V, Seetharami Reddy B, Seshi Reddy T, Lakshminarayana S and Bhuloka Reddy S 2004 Multiple ionization effects on L X-ray intensity ratios in Hf, Ta, Re, Ir, Pt, Au and Pb due to proton bombardment at energies 1-5 MeV *Eur. Phys. J. D* **30** 171
- [19] Uchai W, Lapicki G, Milner W T, Raman S, Rao P V and Vane C R 1985 L X-ray emission from high-Z elements after ionisation by 1 MeV  $u^{-1}$  Ag ions *J. Phys. B* **18** L389
- [20] Ito S, Shoji M, Maeda N, Katano R, Mukoyama T, Ono R, Nakayama Y, P L F, S M T and I, Parente F, Chen M H C B and M H, H S J, Uchai W, Lapicki G, Milner W T, Raman S R P V and V C R and Uchai W, Nestor C W R S and V C R 1987 L  $\gamma$  X-ray emission in heavy-ion bombardment of Bi *J. Phys. B* **20** L597
- [21] Berinde A, Ciortea C, Enulescu A, Fluerasu D, Hock G, Piticu I, Sarkadi L, Sulik B and Zoran V 1987 On the L-M-N multiple ionisation in heavy elements *J. Phys. B* **20** L481
- [22] Braziewicz J, Semaniak J, Czyzewski T, Glowacka L, Jaskola M, Haller M, Karschnick R, Kretschmer W and Trautmann D 1994 L-subshell ionization of rare earth elements by carbon ion bombardment *J. Phys. B* **27** 1535
- [23] Mehta R, Sun H L, Marble D K, Duggan J L, McDaniel F D and Lapicki G 1995 L-shell X-ray production by 2-12 MeV carbon ions in fifteen selected elements from copper to lead *J. Phys. B* **28** 1187
- [24] Yu Y, Wang C, Lin E and Liu T 1997 L x-ray production in lanthanide elements by 1-5 MeV helium ions *J. Phys. B* **30** 5791
- [25] Bogdanović I, Tadić T, Jakšić M, Halabuka Z and Trautmann D 1999 L-shell ionization of Cd, Sb, Te, Ba, La, Eu, Tb and Yb by  $^{16}\text{O}$  ions in the energy range from 0.19 to 0.75 MeV  $u^{-1}$  *Nucl. Instr. Meth. B* **150** 18
- [26] Yu Y C, Azordegan A R, Sun H L, Duggan J L, McDaniel F D, Lin E K, Wang C W and Lapicki G 1999 Charge state dependence of L-shell X-ray production cross sections of  $^{28}\text{Ni}$ ,  $^{29}\text{Cu}$ ,  $^{30}\text{Zn}$ ,  $^{31}\text{Ga}$  and  $^{32}\text{Ge}$  by 12 MeV  $^{16}\text{O}^{q+}$  ions *Nucl. Instr. Meth. B* **150** 27

- [27] Mitra D, Sarkar M, Bhattacharya D, Sen P and Lapicki G 1999 L subshell ionisation cross section of gold by 8-15 MeV Si ions *Nucl. Instr. Meth. B* **152** 207
- [28] Singh Y P, Mitra D, Tribedi L C and Tandon P N 2000 L-subshell ionization of Bi, Au, and Yb induced by F ions at intermediate velocities *Phys. Rev. A* **63** 12713
- [29] Banaś D, Pajek M, Semaniak J, Braziewicz J, Kubala-Kukuś A, Majewska U, Czyżewski T, Jaskóła M, Kretschmer W, Mukoyama T and Trautmann D 2002 Multiple ionization effects in low-resolution X-ray spectra induced by energetic heavy ions *Nucl. Instr. Meth. B* **195** 233
- [30] Banaś D, Braziewicz J, Pajek M, Semaniak J, Czyżewski T, Fijał I, Jaskóła M, Kretschmer W, Mukoyama T and Trautmann D 2002 The role of multiple ionization and subshell coupling effects in L-shell ionization of Au by oxygen ions *J. Phys. B* **35** 3421
- [31] Pajek M, Banaś D, Semaniak J, Braziewicz J, Majewska U, Chojnacki S, Czyżewski T, Fijał I, Jaskóła M, Glombik A, Kretschmer W, Trautmann D, Lapicki G and Mukoyama T 2003 Multiple ionization and coupling effects in L-subshell ionization of heavy atoms by oxygen ions *Phys. Rev. A* **68** 1
- [32] Czarnota M, Banaś D, Berset M, Chmielewska D, Dousse J-C, Hoszowska J, Maillard Y-P, Mauron O, Pajek M, Polasik M, Raboud P A, Rzadkiewicz J, Słabkowska K and Sujkowski Z 2010 High-resolution X-ray study of the multiple ionization of Pd atoms by fast oxygen ions *Eur. Phys. J. D* **57** 321
- [33] Miranda J, Murillo G, Méndez B, López-Monroy J, Díaz R V, Aspiazu J and Villaseñor P 2013 L-shell X-ray production cross sections of selected lanthanoids by impact of  $7\text{Li}^{2+}$  ions with energies between 3.50MeV and 5.25MeV *Radiat. Phys. Chem.* **83** 48
- [34] Murillo G, Méndez B, López-Monroy J, Miranda J and Villaseñor P 2016 L-shell X-ray production cross sections of Ce, Nd, Sm, Eu, Gd, and Dy by impact of  $14\text{N}^{2+}$  ions with energies between 7.0MeV and 10.5MeV *Nucl. Instr. Meths. B* **383** 89
- [35] Kalkal S, Abhilash S R, Kabiraj D, Mandal S, Madhavan N and Singh R 2010 Fabrication of  $90,94\text{Zr}$  targets on carbon backing *Nucl. Instr. Meth. A* **613** 190
- [36] Rozet J P, Stéphan C and Vernhet D 1996 ETACHA: a program for calculating charge states at GANIL energies *Nucl. Instr. Meths. B* **107** 67
- [37] Berger M, Hubbell J, Seltzer S and Chang J 1998 XCOM: photon cross sections database *NIST Stand. Ref.* **8** 3587
- [38] Ziegler J F, Ziegler M D and Biersack J P 2010 SRIM – The stopping and range of ions in matter (2010) *Nucl. Inst. Meths. B* **268** 1818
- [39] Subramaniam E and Kumar B 2010 Data Acquisition Systems-Current and Future

- Trends *DAE Symp. Nucl. Phys* **117**
- [40] Marquardt D W 1963 Algorithm for Least-Squares Estimation of Nonlinear Parameters *J. Soc. Indust. Appl. Math* **11** 431
- [41] Campbell J L and Papp T 2001 Widths of the Atomic K–N7 Levels *At. Data Nucl. Data Tables* **77** 1
- [42] Scofield J H 1973 *Theoretical photoionization cross sections from 1 to 1500 keV, Lawrence Livermore Laboratory Report No, UCRL-51326* (California)
- [43] Campbell J L 2003 Fluorescence yields and Coster – Kronig probabilities for the atomic L subshells q *At. Data Nucl. Data Tables* **85** 291
- [44] Campbell J L 2009 Fluorescence yields and Coster-Kronig probabilities for the atomic L subshells. Part II: The L1 subshell revisited *At. Data Nucl. Data Tables* **95** 115
- [45] Campbell J L and Wang J X 1989 Interpolated Dirac-Fock values of L-subshell x-ray emission rates including overlap and exchange effects *At. Data Nucl. Data Tables* **43** 281
- [46] Sarkadi L and Mukoyamai T 1980 Measurements of L x-ray production and subshell ionisation cross sections of gold by light and heavyion bombardment in the energy range 0 . 4-3-4 MeV *J. Phys B* **13** 2255
- [47] Palinkas J, Sarkadi L, Schlenk B, Torok I, Kalman G, Bauer C, Brankoff K, Grambole D, Heiser C, Rudolph W and Thomas H J 1984 Study of the L-shell ionisation of gold by 3.0-18.2 MeV nitrogen-ion bombardment *J. Phys. B* **17** 131
- [48] Kumar A, Agnihotri A N, Chatterjee S, Kasthurirangan S, Misra D, Choudhury R K, Sarkadi L and Tribedi L C 2010 L3-subshell alignment of Au and Bi in collisions with 12-55-MeV carbon ions *Phys. Rev. A* **81** 62709
- [49] Merzbacher E and Lewis H W 1958 *Handbuch der Physik*, ed S. Flügge (Springer, Berlin) Vol,**38**, p.161.
- [50] Khandelwal G S, Choi B -H, and Merzbacher E 1969 Tables for Born approximation calculations of K and L-shell ionization by protons and other charged particles *At. Data Nucl. Data Tables* **1** 103
- [51] Choi B -H, Merzbacher E and Khandelwal G S 1973 Tables for Born Approximation Calculations of L-Subshell Ionization By Simple Heavy Charged Particles *At. Data Nucl. Data Tables* **5** 291
- [52] Hansen J S 1973 Formulation of the Binary-Encounter Approximation in Configuration Space and its Application to Ionization by Light Ions *Phys. Rev. A* **8** 822
- [53] Hansteen J M and Mosebekk O P 1970 Inner shell ionization by heavy, charged particles

- and associated energy loss of the projectile *Zeit. fur Phys.* **234** 281
- [54] Nikolaev V S 1966 Calculation of the effective cross section for proton charge exchange in multi-electron atoms *Zh.Eksp.Teor.Fiz.* **51** (1966) 1263 [ *Sov. Phys.-1967 JETP.* **24** 847].
- [55] Brandt W and Lapicki G 1981 Energy-loss effect in inner-shell Coulomb ionization by heavy charged particles *Phys. Rev. A* **23** 1717
- [56] Lapicki G 2002 The status of theoretical L-subshell ionization cross sections for protons *Nucl. Instr. Meths. B* **189** 8
- [57] Scofield J H 1974 Relativistic hartree-slater values for K and L X-ray emission rates *At. Data Nucl. Data Tables* **14** 121
- [58] Krause M O 1979 Atomic radiative and radiationless yields for K and L shells *J. Phys. Chem. Ref. Data* **8** 307
- [59] Chen M H, Crasemann B and Mark H 1981 Widths and fluorescence yields of atomic L-shell vacancy states *Phys. Rev. A* **24** 177
- [60] Lapicki G, Mehta R, Duggan J L, Kocur P M, Price J L and McDaniel F D 1986 Multiple outer-shell ionization effect in inner-shell x-ray production by light ions *Phys. Rev. A* **34** 3813
- [61] Mehta R, Duggan J L, Mcdaniel F D, Mcneir M R, Yu Y C, Marble D K and Lapicki G 1993 L-shell X-ray production cross sections for <sup>29</sup>Cu, <sup>31</sup>Ga, <sup>32</sup>Ge, <sup>35</sup>Br, <sup>39</sup>Y, <sup>60</sup>Nd, <sup>64</sup>Gd, <sup>67</sup>Ho, <sup>70</sup>Yb, <sup>79</sup>Au, and <sup>82</sup>Pb for 2-25 MeV carbon ions *Nucl. Instr. Meths. B* **79** 175
- [62] Sarkadi L 1986 L3-subshell alignment calculations in the second-order Born approximation for light- and heavy-ion impact on Au *J. Phys. B At. Mol. Phys.* **19** 2519
- [63] Sarkar M, Bhattacharya D, Chatterjee M B, Sen P, Kuri G, Mahapatra D P and Lapicki G 1995 Importance of subshell coupling in L-shell ionization by low-velocity heavy ions *Nucl. Instr. Meth. B* **103** 23
- [64] Lapicki G, Ramana Murty G A V., Naga Raju G J, Reddy B S, Reddy S B and Vijayan V 2004 Effects of multiple ionization and intrashell coupling in L-subshell ionization by heavy ions *Phys. Rev. A* **70** 62718

**Table 1.** The L $\alpha$ , L $\beta$ , L $\gamma$ , and total L x-ray production cross section (barn) in elements with  $78 \leq Z_T \leq 92$  for incident  $^{19}\text{F}$  ions as measured and calculated with ionization cross sections according to the FBA [49–51,54], ECPSSR [55], and ECUSAR [56] converted to x-ray production cross sections with atomic parameters modified for multiply-ionized (MI) elements [60]. The ratios of the measured to calculated cross sections are listed in the parenthesis. In bold print are the best ratios. With  $q = 6^+$  and  $7^+$ , the ratios of the data to ECUSAR-MI and ECPSSR-MI are (within 15% uncertainties of our measurements) statistically similar, while the ECUSAR-MI are definitely in closer agreement with the measurements than ECPSSR-MI above 100 MeV and  $q = 8^+$ .

Element	$^{19}\text{F}$ ion beam		x-ray production cross sections (barn)			
	Energy (MeV)	Charge q	Measured	ECUSAR-MI	ECPSSR-MI	FBA-MI
$^{78}\text{Pt}$						
L $\alpha$ x-ray	76	$6^+$	206	207( <b>1.00</b> )	203(1.01)	417(0.49)
	84	$6^+$	226	253(0.89)	249( <b>0.91</b> )	474(0.48)
	90	$7^+$	260	296(0.88)	291( <b>0.89</b> )	534(0.49)
	98	$8^+$	323	372(0.87)	347( <b>0.93</b> )	678(0.48)
	106	$8^+$	423	425( <b>1.00</b> )	385(1.10)	737(0.57)
	114	$8^+$	416	477(0.87)	448( <b>0.93</b> )	794(0.52)
L $\beta$ x-ray	76	$6^+$	4449	4166( <b>1.07</b> )	4092(1.09)	8411(0.53)
	84	$6^+$	4685	5110(0.92)	5018( <b>0.93</b> )	9567(0.49)
	90	$7^+$	5749	5975(0.96)	5863( <b>0.98</b> )	10768(0.53)
	98	$8^+$	7015	7507(0.93)	7009( <b>1.00</b> )	13677(0.51)
	106	$8^+$	8602	8568( <b>1.00</b> )	7758(1.11)	14872(0.58)
	114	$8^+$	8811	9624( <b>0.92</b> )	8045(1.10)	16008(0.55)
L $\gamma$ x-ray	76	$6^+$	2532	2373( <b>1.07</b> )	2339(1.08)	5169(0.49)
	84	$6^+$	3037	2962( <b>1.03</b> )	2919(1.04)	5940(0.51)
	90	$7^+$	3613	3517( <b>1.03</b> )	3463(1.04)	6826(0.53)
	98	$8^+$	4338	4466(0.971)	4219( <b>1.028</b> )	8593(0.50)
	106	$8^+$	5507	5169( <b>1.07</b> )	4713(1.17)	9482(0.58)
	114	$8^+$	6007	5879( <b>1.02</b> )	5576(1.08)	10340(0.58)



	90	7 <sup>+</sup>	481	521(0.92)	514( <b>0.94</b> )	1051(0.46)
	98	8 <sup>+</sup>	598	667(0.90)	636( <b>0.94</b> )	1315(0.45)
	106	8 <sup>+</sup>	804	780( <b>1.03</b> )	715(1.12)	1466(0.55)
	114	8 <sup>+</sup>	883	895( <b>0.99</b> )	855(1.03)	1615(0.55)
Total L						
	76	6 <sup>+</sup>	7533	7087( <b>1.06</b> )	6971(1.08)	14773(0.51)
	84	6 <sup>+</sup>	8377	8758(0.96)	8614( <b>0.97</b> )	16880(0.50)
	90	7 <sup>+</sup>	10103	10309(0.98)	10131( <b>1.00</b> )	19180(0.53)
	98	8 <sup>+</sup>	12274	13012(0.94)	12211( <b>1.01</b> )	24263(0.51)
	106	8 <sup>+</sup>	15337	14941( <b>1.03</b> )	13571(1.13)	26558(0.58)
	114	8 <sup>+</sup>	16117	16876(0.96)	15924( <b>1.01</b> )	28755(0.56)
<sup>79</sup> Au						
Ll x-ray						
	76	6 <sup>+</sup>	182	193(0.94)	189( <b>0.96</b> )	395(0.46)
	84	6 <sup>+</sup>	220	237(0.93)	233( <b>0.94</b> )	450(0.49)
	90	7 <sup>+</sup>	270	278(0.97)	273( <b>0.99</b> )	508(0.53)
	98	8 <sup>+</sup>	323	349(0.93)	327( <b>0.99</b> )	643(0.50)
	106	8 <sup>+</sup>	453	400( <b>1.13</b> )	363(1.25)	701(0.65)
	114	8 <sup>+</sup>	463	451( <b>1.03</b> )	424(1.09)	757(0.61)
L $\alpha$ x-ray						
	76	6 <sup>+</sup>	3854	3829( <b>1.01</b> )	3765(1.02)	7849(0.49)
	84	6 <sup>+</sup>	3921	4713(0.83)	4634( <b>0.85</b> )	8952(0.44)
	90	7 <sup>+</sup>	5344	5521(0.97)	5421( <b>0.99</b> )	10097(0.53)
	98	8 <sup>+</sup>	6416	6939(0.93)	6498( <b>0.99</b> )	12775(0.50)
	106	8 <sup>+</sup>	8632	7948( <b>1.09</b> )	7210(1.20)	13940(0.62)
	114	8 <sup>+</sup>	9574	8958( <b>1.07</b> )	8437(1.13)	15054(0.64)
L $\beta$ x-ray						
	76	6 <sup>+</sup>	2169	2160( <b>1.00</b> )	2130(1.03)	4776(0.45)
	84	6 <sup>+</sup>	2397	2704(0.89)	2667( <b>0.90</b> )	5504(0.44)
	90	7 <sup>+</sup>	3265	3216( <b>1.02</b> )	3168(1.03)	6333(0.52)

	98	8 <sup>+</sup>	3850	4084(0.94)	3868( <b>1.00</b> )	7945(0.48)
	106	8 <sup>+</sup>	5382	4742( <b>1.13</b> )	4331(1.24)	8792(0.61)
	114	8 <sup>+</sup>	6224	5411( <b>1.15</b> )	5141(1.21)	9614(0.65)
Ly $\alpha$ -ray						
	76	6 <sup>+</sup>	294	313(0.94)	309( <b>0.95</b> )	723(0.41)
	84	6 <sup>+</sup>	276	398(0.69)	393( <b>0.70</b> )	839(0.33)
	90	7 <sup>+</sup>	441	479(0.92)	473( <b>0.93</b> )	983(0.45)
	98	8 <sup>+</sup>	720	614( <b>1.17</b> )	587(1.23)	1225(0.59)
	106	8 <sup>+</sup>	791	721( <b>1.10</b> )	662(1.19)	1371(0.58)
	114	8 <sup>+</sup>	987	830( <b>1.19</b> )	794(1.24)	1513(0.65)
Total L						
	76	6 <sup>+</sup>	6499	6494( <b>1.00</b> )	6394(1.02)	13742(0.47)
	84	6 <sup>+</sup>	6814	8052(0.85)	7928( <b>0.86</b> )	15746(0.43)
	90	7 <sup>+</sup>	9319	9493(0.98)	9335( <b>1.00</b> )	17920(0.52)
	98	8 <sup>+</sup>	11309	11987(0.94)	11279( <b>1.00</b> )	22587(0.50)
	106	8 <sup>+</sup>	15258	13811( <b>1.14</b> )	12565(1.21)	24804(0.62)
	114	8 <sup>+</sup>	17249	15649( <b>1.10</b> )	14797(1.17)	26938(0.64)
<sup>82</sup> Pb						
Ll x-ray						
	76	6 <sup>+</sup>	152	138(1.10)	151( <b>1.01</b> )	327(0.46)
	84	6 <sup>+</sup>	163	189(0.86)	187( <b>0.87</b> )	375(0.43)
	90	7 <sup>+</sup>	215	223(0.96)	219( <b>0.98</b> )	425(0.51)
	98	8 <sup>+</sup>	260	280(0.93)	264( <b>0.98</b> )	533(0.49)
	106	8 <sup>+</sup>	370	324( <b>1.14</b> )	295(1.25)	586(0.63)
	114	8 <sup>+</sup>	325	367(0.89)	348( <b>0.93</b> )	637(0.51)
L $\alpha$ x-ray						
	76	6 <sup>+</sup>	3010	2611(1.15)	2858( <b>1.05</b> )	6206(0.49)
	84	6 <sup>+</sup>	3000	3595(0.83)	3539( <b>0.85</b> )	7122(0.42)
	90	7 <sup>+</sup>	4202	4228( <b>0.994</b> )	4159(1.010)	8057(0.52)
	98	8 <sup>+</sup>	4794	5321(0.90)	5015( <b>0.96</b> )	10110(0.47)
	106	8 <sup>+</sup>	6747	6140( <b>1.10</b> )	5593(1.21)	11110(0.61)
	114	8 <sup>+</sup>	6799	6971( <b>0.98</b> )	6596(1.03)	12077(0.56)
L $\beta$ x-ray						

	76	6 <sup>+</sup>	1662	1559(1.07)	1605( <b>1.04</b> )	3752(0.44)
	84	6 <sup>+</sup>	1743	2048(0.85)	2022( <b>0.86</b> )	4354(0.40)
	90	7 <sup>+</sup>	2455	2445( <b>1.00</b> )	2412(1.02)	5021(0.49)
	98	8 <sup>+</sup>	2886	3108(0.93)	2961( <b>0.97</b> )	6247(0.46)
	106	8 <sup>+</sup>	4112	3637( <b>1.13</b> )	3334(1.23)	6962(0.59)
	114	8 <sup>+</sup>	4415	4181( <b>1.06</b> )	3993(1.11)	7665(0.58)
L $\gamma$ x-ray						
	76	6 <sup>+</sup>	216	236(0.915)	234( <b>0.923</b> )	572(0.38)
	84	6 <sup>+</sup>	212	302(0.70)	299( <b>0.71</b> )	670(0.32)
	90	7 <sup>+</sup>	371	366( <b>1.01</b> )	362(1.02)	787(0.47)
	98	8 <sup>+</sup>	398	470(0.85)	451( <b>0.88</b> )	973(0.41)
	106	8 <sup>+</sup>	587	556( <b>1.06</b> )	512(1.15)	1097(0.54)
	114	8 <sup>+</sup>	647	646( <b>1.00</b> )	622(1.04)	1220(0.53)
Total L						
	76	6 <sup>+</sup>	5039	4544(1.11)	4848( <b>1.04</b> )	10858(0.46)
	84	6 <sup>+</sup>	5118	6135(0.83)	6047( <b>0.85</b> )	12522(0.41)
	90	7 <sup>+</sup>	7242	7262( <b>1.00</b> )	7152(1.01)	14290(0.51)
	98	8 <sup>+</sup>	8338	9180(0.91)	8692( <b>0.96</b> )	17862(0.47)
	106	8 <sup>+</sup>	11816	10658( <b>1.11</b> )	9734(1.21)	19754(0.60)
	114	8 <sup>+</sup>	12186	12165( <b>1.00</b> )	11558(1.05)	21598(0.56)
<sup>83</sup> Bi						
L $\lambda$ x-ray						
	76	6 <sup>+</sup>	172	142( <b>1.21</b> )	140(1.23)	307(0.56)
	84	6 <sup>+</sup>	162	176(0.92)	173( <b>0.94</b> )	353(0.46)
	90	7 <sup>+</sup>	181	207(0.87)	204( <b>0.89</b> )	400(0.45)
	98	8 <sup>+</sup>	259	261( <b>0.99</b> )	246(1.05)	500(0.52)
	106	8 <sup>+</sup>	361	301( <b>1.12</b> )	275(1.31)	551(0.66)
	114	8 <sup>+</sup>	311	343(0.91)	325( <b>0.96</b> )	600(0.52)
L $\alpha$ x-ray						
	76	6 <sup>+</sup>	2963	2648( <b>1.12</b> )	2610(1.14)	5744(0.52)
	84	6 <sup>+</sup>	2860	3287(0.87)	3238( <b>0.88</b> )	6603(0.43)
	90	7 <sup>+</sup>	3428	3871(0.89)	3811( <b>0.90</b> )	7476(0.46)
	98	8 <sup>+</sup>	4730	4873(0.971)	4602( <b>1.028</b> )	9355(0.51)
	106	8 <sup>+</sup>	6015	5635( <b>1.07</b> )	5138(1.17)	10301(0.58)
	114	8 <sup>+</sup>	6557	6411( <b>1.02</b> )	6075(1.08)	11220(0.58)

L $\beta$  x-ray

76	6 <sup>+</sup>	1630	1480( <b>1.10</b> )	1462(1.11)	3465(0.47)
84	6 <sup>+</sup>	1648	1868(0.88)	1845( <b>0.89</b> )	4028(0.41)
90	7 <sup>+</sup>	2049	2232(0.92)	2203( <b>0.93</b> )	4648(0.44)
98	8 <sup>+</sup>	2746	2839(0.97)	2709( <b>1.01</b> )	5767(0.48)
106	8 <sup>+</sup>	3638	3329( <b>1.09</b> )	3055(1.19)	6441(0.56)
114	8 <sup>+</sup>	4253	3836( <b>1.11</b> )	3668(1.16)	7106(0.60)

L $\gamma$  x-ray

76	6 <sup>+</sup>	213	215(0.99)	213( <b>1.00</b> )	530(0.40)
84	6 <sup>+</sup>	190	276(0.688)	274( <b>0.693</b> )	622(0.31)
90	7 <sup>+</sup>	255	335(0.76)	331( <b>0.77</b> )	731(0.35)
98	8 <sup>+</sup>	374	430(0.87)	414( <b>0.90</b> )	902(0.41)
106	8 <sup>+</sup>	657	511( <b>1.29</b> )	471(1.39)	1019(0.64)
114	8 <sup>+</sup>	596	595( <b>1.00</b> )	573(1.04)	1137(0.52)

Total L

76	6 <sup>+</sup>	4978	4485( <b>1.11</b> )	4425(1.12)	10046(0.50)
84	6 <sup>+</sup>	4859	5607(0.87)	5530( <b>0.88</b> )	11607(0.42)
90	7 <sup>+</sup>	5913	6645(0.89)	6550( <b>0.90</b> )	13255(0.45)
98	8 <sup>+</sup>	8109	8402(0.97)	7972( <b>1.02</b> )	16525(0.49)
106	8 <sup>+</sup>	10671	9776( <b>1.09</b> )	8940(1.19)	18313(0.58)
114	8 <sup>+</sup>	11717	11185( <b>1.05</b> )	10642(1.10)	20064(0.58)

<sup>90</sup>Th

L $\iota$  x-ray

76	6 <sup>+</sup>	86	85( <b>1.01</b> )	84(1.02)	203(0.42)
84	6 <sup>+</sup>	108	106( <b>1.02</b> )	105(1.03)	235(0.46)
90	7 <sup>+</sup>	148	126( <b>1.17</b> )	125(1.18)	267(0.55)
98	8 <sup>+</sup>	144	159(0.91)	152( <b>0.95</b> )	328(0.44)
106	8 <sup>+</sup>	204	186( <b>1.10</b> )	171(1.19)	366(0.56)
114	8 <sup>+</sup>	297	213( <b>1.39</b> )	205(1.45)	403(0.74)

L $\alpha$  x-ray

76	6 <sup>+</sup>	1365	1416(0.96)	1401( <b>0.97</b> )	3378(0.40)
84	6 <sup>+</sup>	1510	1775(0.85)	1755( <b>0.86</b> )	3923(0.38)
90	7 <sup>+</sup>	2411	2104( <b>1.15</b> )	2078(1.16)	4457(0.54)
98	8 <sup>+</sup>	2453	2646(0.93)	2534( <b>0.97</b> )	5470(0.45)
106	8 <sup>+</sup>	3375	3099( <b>1.09</b> )	2854(1.18)	6095(0.55)
114	8 <sup>+</sup>	3717	3554( <b>1.05</b> )	3421(1.09)	6716(0.55)

L $\beta$  x-ray

	76	6 <sup>+</sup>	757	762(0.99)	755( <b>1.00</b> )	1960(0.39)
	84	6 <sup>+</sup>	807	970(0.83)	961( <b>0.84</b> )	2297(0.35)
	90	7 <sup>+</sup>	1313	1165( <b>1.13</b> )	1153(1.14)	2662(0.49)
	98	8 <sup>+</sup>	1346	1479(0.91)	1430( <b>0.94</b> )	3249(0.41)
	106	8 <sup>+</sup>	1860	1757( <b>1.06</b> )	1628(1.14)	3672(0.51)
	114	8 <sup>+</sup>	2125	2034( <b>1.05</b> )	1983(1.07)	4098(0.52)
L $\gamma$ x-ray						
	76	6 <sup>+</sup>	109	109( <b>1.00</b> )	108(1.01)	299(0.36)
	84	6 <sup>+</sup>	114	141(0.809)	140( <b>0.814</b> )	353(0.32)
	90	7 <sup>+</sup>	200	172( <b>1.16</b> )	171(1.17)	418(0.48)
	98	8 <sup>+</sup>	192	221(0.87)	216( <b>0.89</b> )	508(0.38)
	106	8 <sup>+</sup>	302	267( <b>1.13</b> )	248(1.22)	582(0.52)
	114	8 <sup>+</sup>	340	311( <b>1.09</b> )	308(1.10)	658(0.52)
Total L						
	76	6 <sup>+</sup>	2318	2371(0.98)	2348( <b>0.99</b> )	5839(0.40)
	84	6 <sup>+</sup>	2538	2993(0.85)	2961( <b>0.86</b> )	6808(0.37)
	90	7 <sup>+</sup>	4072	3566( <b>1.14</b> )	3527(1.15)	7804(0.52)
	98	8 <sup>+</sup>	4136	4505(0.92)	4332( <b>0.95</b> )	9556(0.43)
	106	8 <sup>+</sup>	5742	5309( <b>1.08</b> )	4901(1.17)	10715(0.54)
	114	8 <sup>+</sup>	6479	6112( <b>1.06</b> )	5918(1.09)	11876(0.55)
 <sup>92</sup> U						
L $\iota$ x-ray						
	76	6 <sup>+</sup>	97	75( <b>1.29</b> )	74(1.31)	183(0.53)
	84	6 <sup>+</sup>	91	94(0.97)	93( <b>0.98</b> )	213(0.43)
	90	7 <sup>+</sup>	194	111( <b>1.75</b> )	110(1.76)	242(0.80)
	98	8 <sup>+</sup>	203	140( <b>1.45</b> )	134(1.51)	296(0.69)
	106	8 <sup>+</sup>	262	164( <b>1.60</b> )	152(1.72)	330(0.79)
	114	8 <sup>+</sup>	293	190( <b>1.54</b> )	182(1.61)	365(0.80)
L $\alpha$ x-ray						
	76	6 <sup>+</sup>	1113	1205(0.92)	1192( <b>0.93</b> )	2955(0.38)
	84	6 <sup>+</sup>	1250	1513(0.83)	1497( <b>0.84</b> )	3439(0.36)
	90	7 <sup>+</sup>	1997	1795( <b>1.11</b> )	1774(1.13)	3906(0.51)
	98	8 <sup>+</sup>	2201	2255(0.976)	2168( <b>1.015</b> )	4767(0.46)
	106	8 <sup>+</sup>	2871	2649( <b>1.08</b> )	2446(1.17)	5325(0.54)
	114	8 <sup>+</sup>	3184	3060( <b>1.04</b> )	2942(1.08)	5883(0.54)
L $\beta$ x-ray						

	76	6 <sup>+</sup>	603	625(0.965)	620( <b>0.973</b> )	1650(0.37)
	84	6 <sup>+</sup>	622	798(0.78)	791( <b>0.79</b> )	1944(0.32)
	90	7 <sup>+</sup>	1084	959( <b>1.13</b> )	950(1.14)	2244(0.48)
	98	8 <sup>+</sup>	1215	1217( <b>1.00</b> )	1180(1.03)	2730(0.45)
	106	8 <sup>+</sup>	1605	1450( <b>1.11</b> )	1345(1.19)	3091(0.52)
	114	8 <sup>+</sup>	1758	1697( <b>1.04</b> )	1645(1.07)	3459(0.51)
L $\gamma$ x-ray						
	76	6 <sup>+</sup>	79	86( <b>0.92</b> )	86( <b>0.92</b> )	244(0.32)
	84	6 <sup>+</sup>	73	112(0.65)	111( <b>0.66</b> )	291(0.25)
	90	7 <sup>+</sup>	174	137( <b>1.27</b> )	136(1.28)	342(0.51)
	98	8 <sup>+</sup>	179	176( <b>1.02</b> )	172(1.04)	416(0.43)
	106	8 <sup>+</sup>	246	213( <b>1.15</b> )	199(1.24)	478(0.51)
	114	8 <sup>+</sup>	275	254( <b>1.08</b> )	248(1.11)	542(0.51)
Total L						
	76	6 <sup>+</sup>	1893	1991(0.95)	1972( <b>0.96</b> )	5032(0.38)
	84	6 <sup>+</sup>	2036	2517(0.81)	2492( <b>0.82</b> )	5887(0.35)
	90	7 <sup>+</sup>	3450	3003( <b>1.15</b> )	2970(1.16)	6734(0.51)
	98	8 <sup>+</sup>	3798	3789( <b>1.00</b> )	3654(1.04)	8208(0.46)
	106	8 <sup>+</sup>	4984	4476( <b>1.11</b> )	4141(1.20)	9224(0.54)
	114	8 <sup>+</sup>	5509	5201( <b>1.06</b> )	5017(1.10)	10249(0.54)

**Table 2.** Fluorescence and CK yields for singly-ionized elements. Values listed as recommended by Campbell [43,44] are used in the present work.

Element	Fluorescence yield								
	$\omega_1^0$			$\omega_2^0$			$\omega_3^0$		
	Campbell [43,44]	Krause [58]	Chen et al [59]	Campbell [43,44]	Krause [58]	Chen et al [59]	Campbell [43,44]	Krause [58]	Chen et al [59]
<sup>78</sup> Pt	0.114	0.114	0.074	0.344	0.321	0.344	0.303	0.306	0.303
<sup>79</sup> Au	0.117	0.107	0.078	0.358	0.334	0.358	0.313	0.320	0.313
<sup>82</sup> Pb	0.128	0.112	0.093	0.397	0.373	0.397	0.343	0.360	0.343
<sup>83</sup> Bi	0.132	0.117	0.098	0.411	0.387	0.411	0.353	0.373	0.353
<sup>90</sup> Th	0.159	0.161	0.139	0.503	0.479	0.503	0.424	0.463	0.424

${}_{92}\text{U}$	0.168	0.176	0.149	0.506	0.467	0.506	0.444	0.489	0.444
-------------------	-------	-------	-------	-------	-------	-------	-------	-------	-------

Element	CK yield								
	$f_{13}^0$			$f_{12}^0$			$f_{23}^0$		
	Campbell [43,44]	Krause [58]	Chen et al [59]	Campbell [43,44]	Krause [58]	Chen et al [59]	Campbell [43,44]	Krause [58]	Chen et al [59]
${}_{78}\text{Pt}$	0.545	0.500	0.716	0.075	0.140	0.067	0.126	0.124	0.132
${}_{79}\text{Au}$	0.615	0.530	0.711	0.074	0.140	0.068	0.125	0.122	0.129
${}_{82}\text{Pb}$	0.620	0.580	0.708	0.066	0.120	0.054	0.119	0.116	0.123
${}_{83}\text{Bi}$	0.620	0.580	0.703	0.063	0.110	0.055	0.117	0.113	0.121
${}_{90}\text{Th}$	0.620	0.570	0.659	0.040	0.090	0.058	0.103	0.108	0.106
${}_{92}\text{U}$	0.620	0.570	0.660	0.035	0.080	0.051	0.140	0.167	0.139

**Table 3.** Fluorescence and CK yields for singly-ionized [43,44] and the ratios of atomic parameters for multiply-ionized [60] to these singly-ionized for  ${}_{78}\text{Pt}$  and  ${}_{92}\text{U}$ .

Ion beam		Fluorescence yield			CK yield		
Energy (MeV)	Charge state q	$\omega_1$	$\omega_2$	$\omega_3$	$f_{13}$	$f_{12}$	$f_{23}$
<i>Singly-ionized <math>{}_{78}\text{Pt}</math></i>							
		0.114	0.344	0.303	0.545	0.075	0.126

Ratios of atomic parameters for multiply [60] to singly [43,44] ionized  ${}_{78}\text{Pt}$

76	$6^+$	1.123	1.087	1.096	0.767	0.773	0.770
84	$6^+$	1.114	1.078	1.086	0.789	0.787	0.786
90	$7^+$	1.140	1.102	1.109	0.736	0.733	0.738
98	$8^+$	1.175	1.125	1.135	0.688	0.693	0.690

106	8 <sup>+</sup>	1.167	1.116	1.122	0.710	0.707	0.706
114	8 <sup>+</sup>	1.149	1.108	1.116	0.728	0.733	0.730

Singly- ionized  ${}_{92}\text{U}$

0.168	0.506	0.444	0.620	0.035	0.140
-------	-------	-------	-------	-------	-------

Ratios of atomic parameters for multiply [60] to singly [43,44] ionized  ${}_{92}\text{U}$

76	6 <sup>+</sup>	1.11	1.07	1.07	0.77	0.77	0.77
84	6 <sup>+</sup>	1.10	1.06	1.07	0.80	0.79	0.79
90	7 <sup>+</sup>	1.14	1.08	1.09	0.74	0.74	0.74
98	8 <sup>+</sup>	1.17	1.09	1.11	0.69	0.69	0.69
106	8 <sup>+</sup>	1.15	1.08	1.10	0.71	0.71	0.71
114	8 <sup>+</sup>	1.14	1.08	1.09	0.74	0.73	0.71

**Table 4.** Standard deviation of the theoretical estimates for singly (SI) and multiply (MI) ionized atoms with respect to measured values. The average standard deviation over all six target elements is also given.

Theory	Target	Standard deviation of theories from the present experimental results				
		Ll	L $\alpha$	L $\beta$	L $\gamma$	L-Total
ECPSSR-SI	Pt	20.4	15.9	20.2	17.1	17.1
	Au	19.5	18.8	21.5	23.2	19.9
	Pb	23.0	18.8	19.8	15.8	18.9
	Bi	34.3	18.8	19.6	27.2	19.5
	Th	22.7	17.3	15.5	18.5	16.8
	U	43.7	16.1	17.6	20.9	18.2
	Average	27.3	17.6	19.0	20.5	18.4
ECUSAR-SI	Pt	18.5	14.6	22.1	19.9	17.5
	Au	16.3	15.9	19.2	21.4	17.3
	Pb	19.8	16.3	17.2	13.4	16.2
	Bi	29.8	15.4	17.0	24.3	16.3
	Th	21.6	14.9	13.3	16.6	14.6
	U	42.6	14.1	15.2	18.8	16.0
	Average	24.8	15.2	17.3	19.0	16.3
ECPSSR -MI	Pt	21.8	9.5	11.1	9.7	8.9
	Au	14.4	14.0	15.5	17.3	14.5
	Pb	19.3	14.2	13.8	12.3	13.7



ECUSAR-MI	Bi	28.5	13.6	13.7	23.7	14.0
	Th	19.5	12.7	10.8	13.8	12.2
	U	40.0	11.8	12.7	16.2	13.4
	Average	23.9	12.6	12.9	15.5	12.8
	Pt	25.3	10.3	5.1	8.0	6.1
	Au	9.3	9.5	11.1	14.1	9.8
	Pb	17.2	11.8	9.8	11.4	10.4
	Bi	23.4	9.3	10.6	20.9	9.6
	Th	17.3	9.6	8.7	11.9	9.4
	U	37.1	8.5	9.7	14.0	10
	Average	21.6	9.8	9.7	13.4	9.2

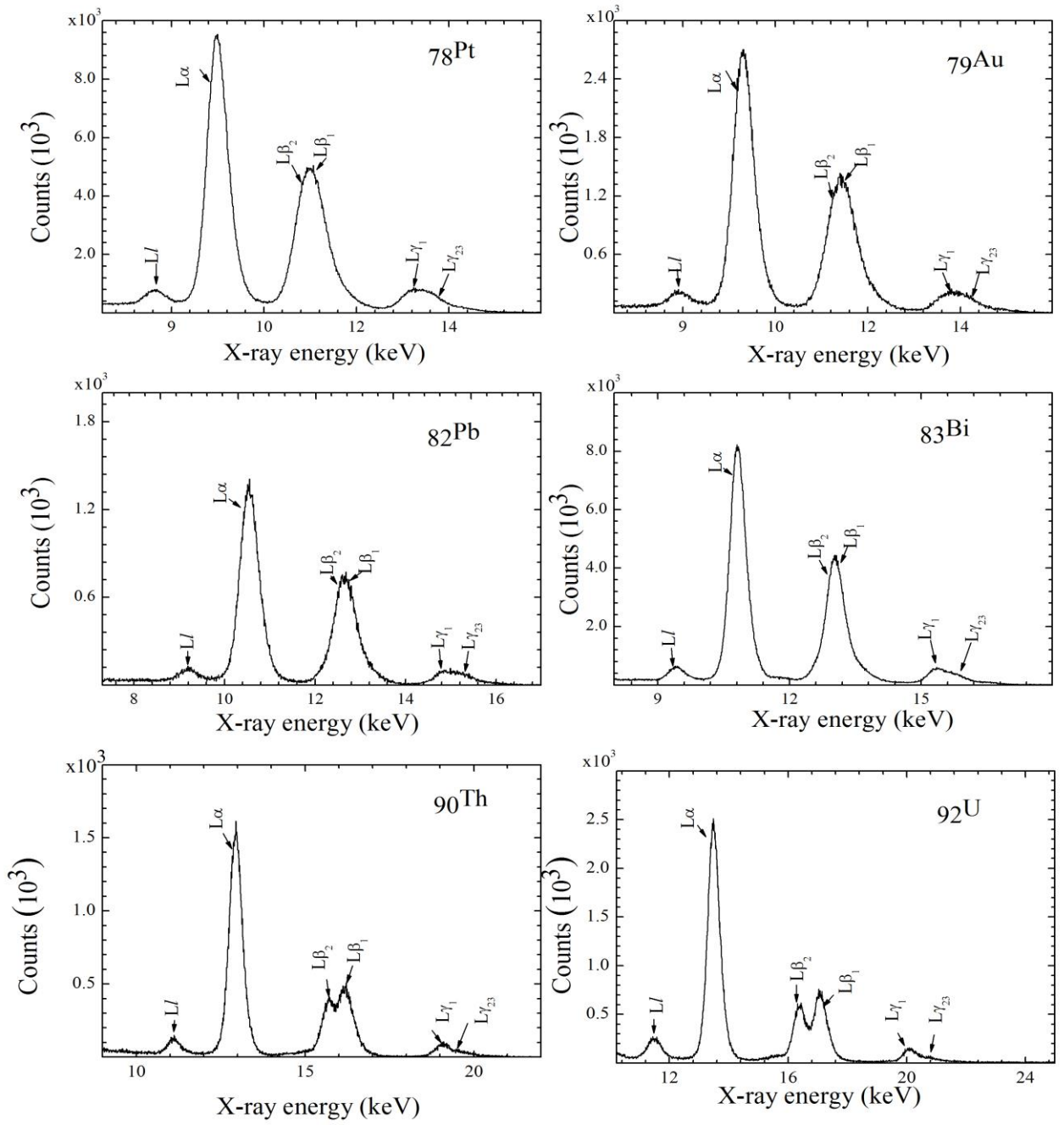


Figure 1

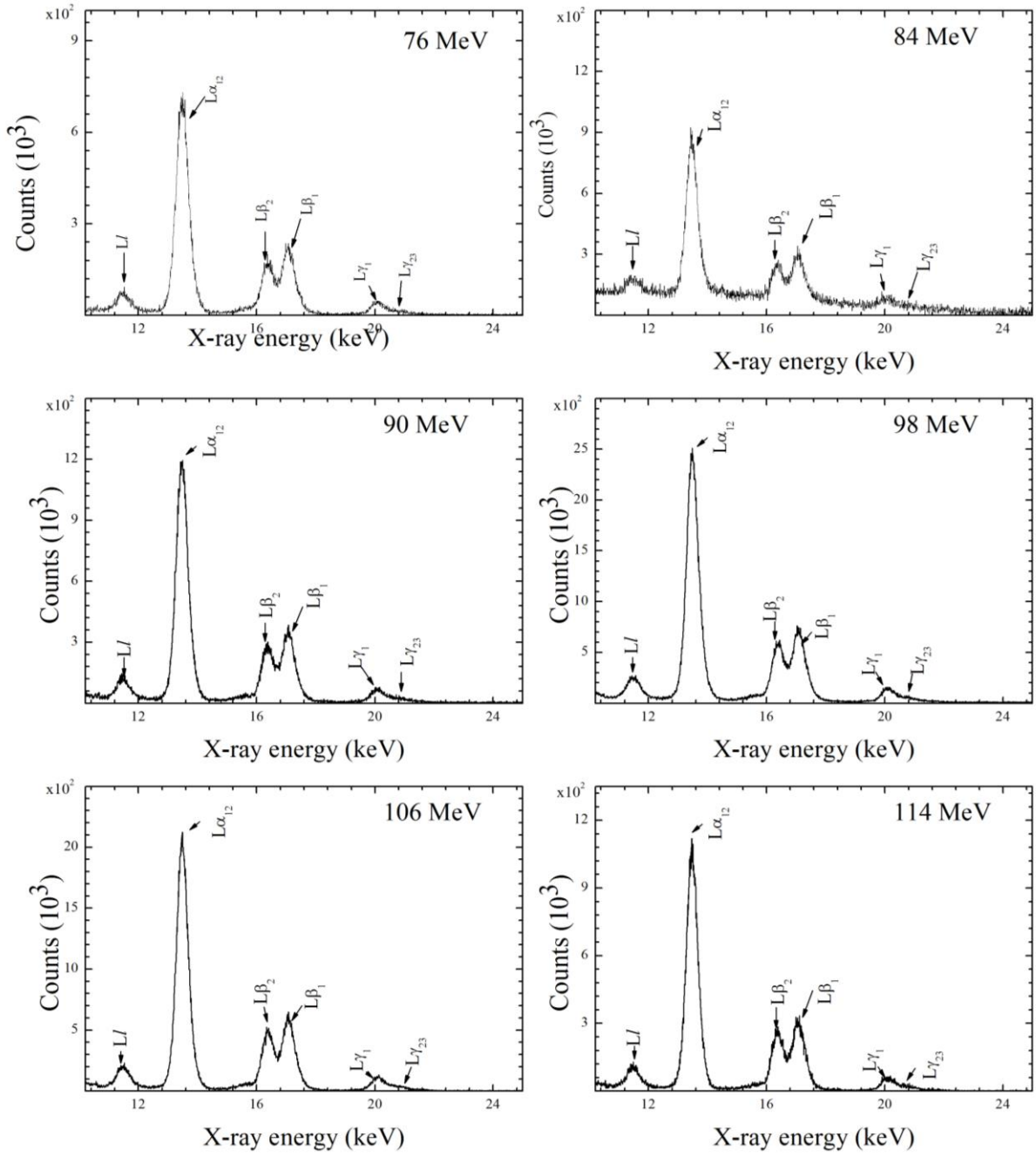


Figure 2

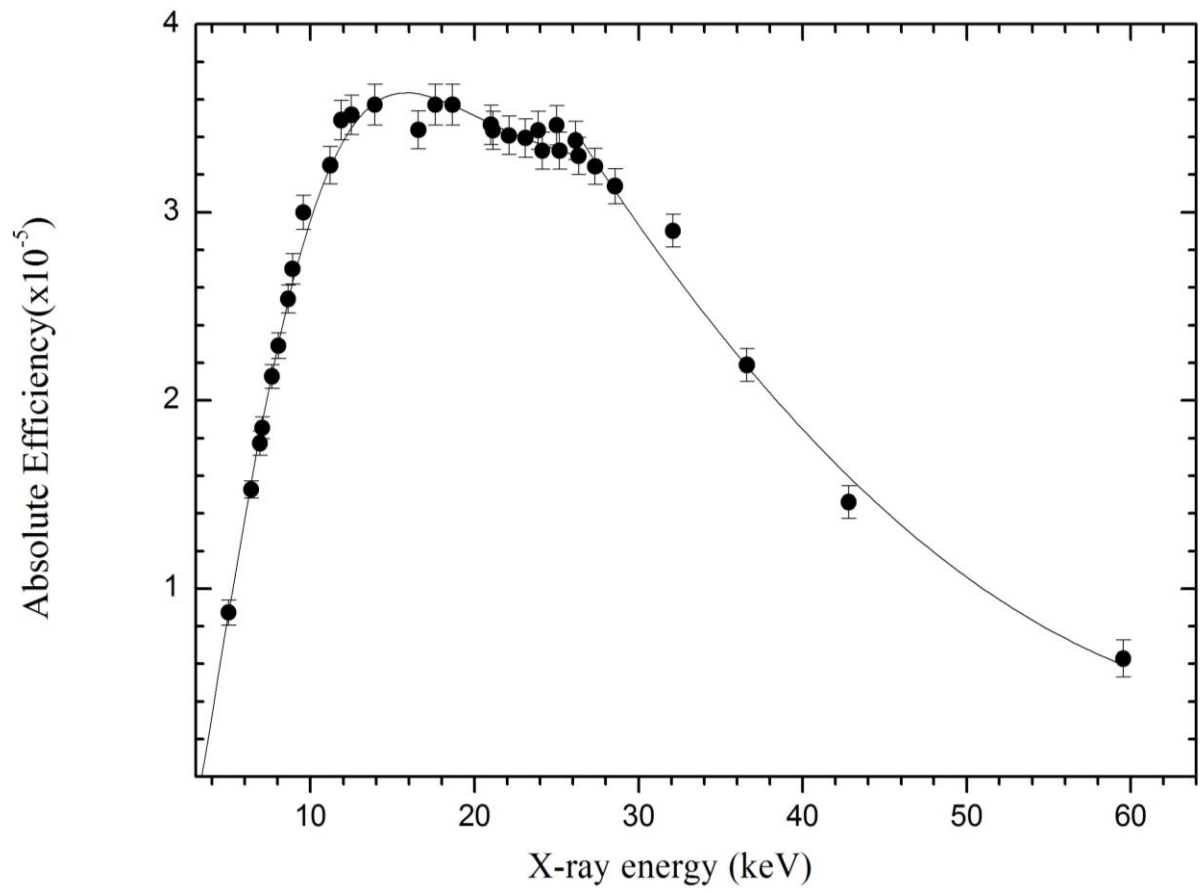


Figure 3

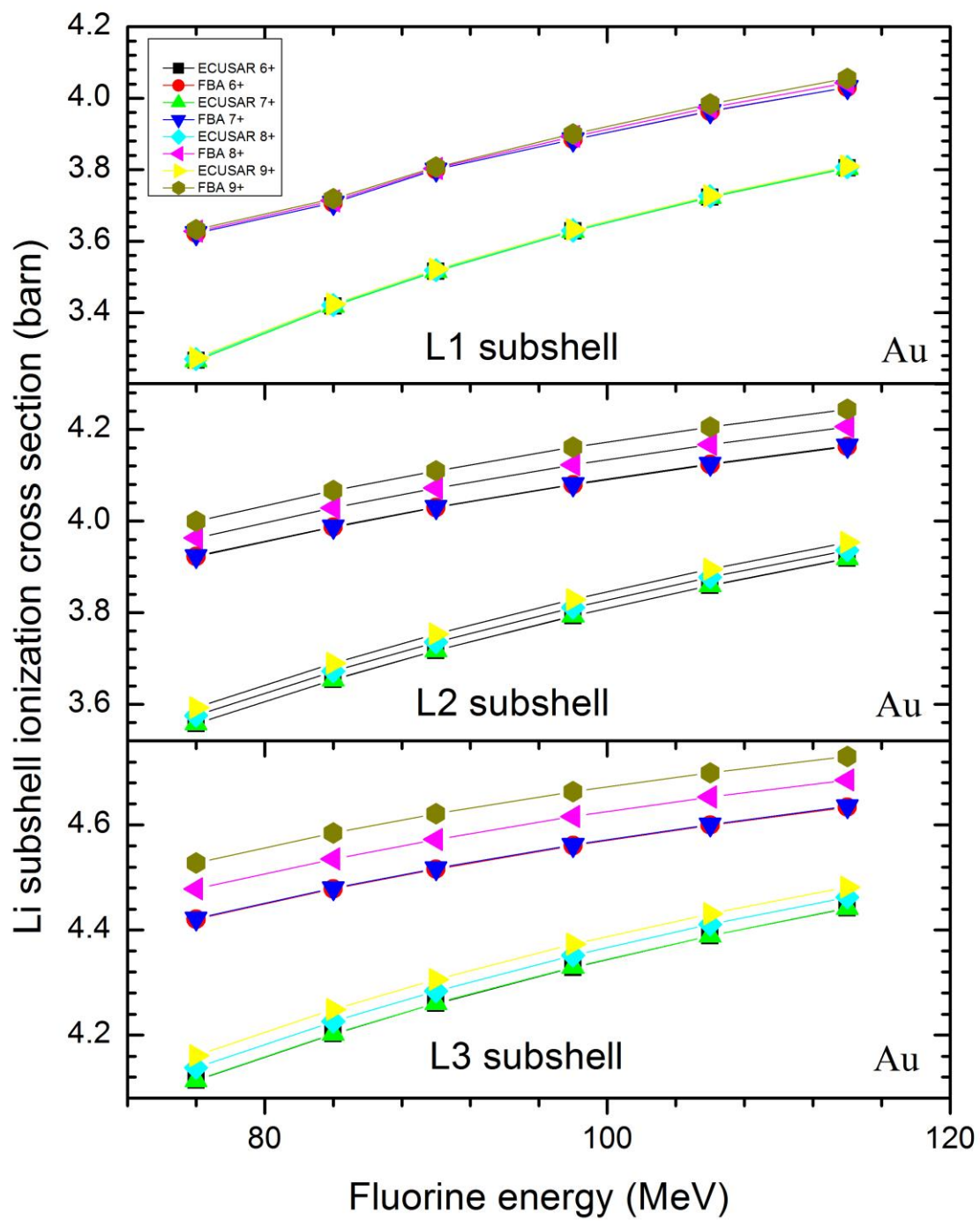


Figure 4

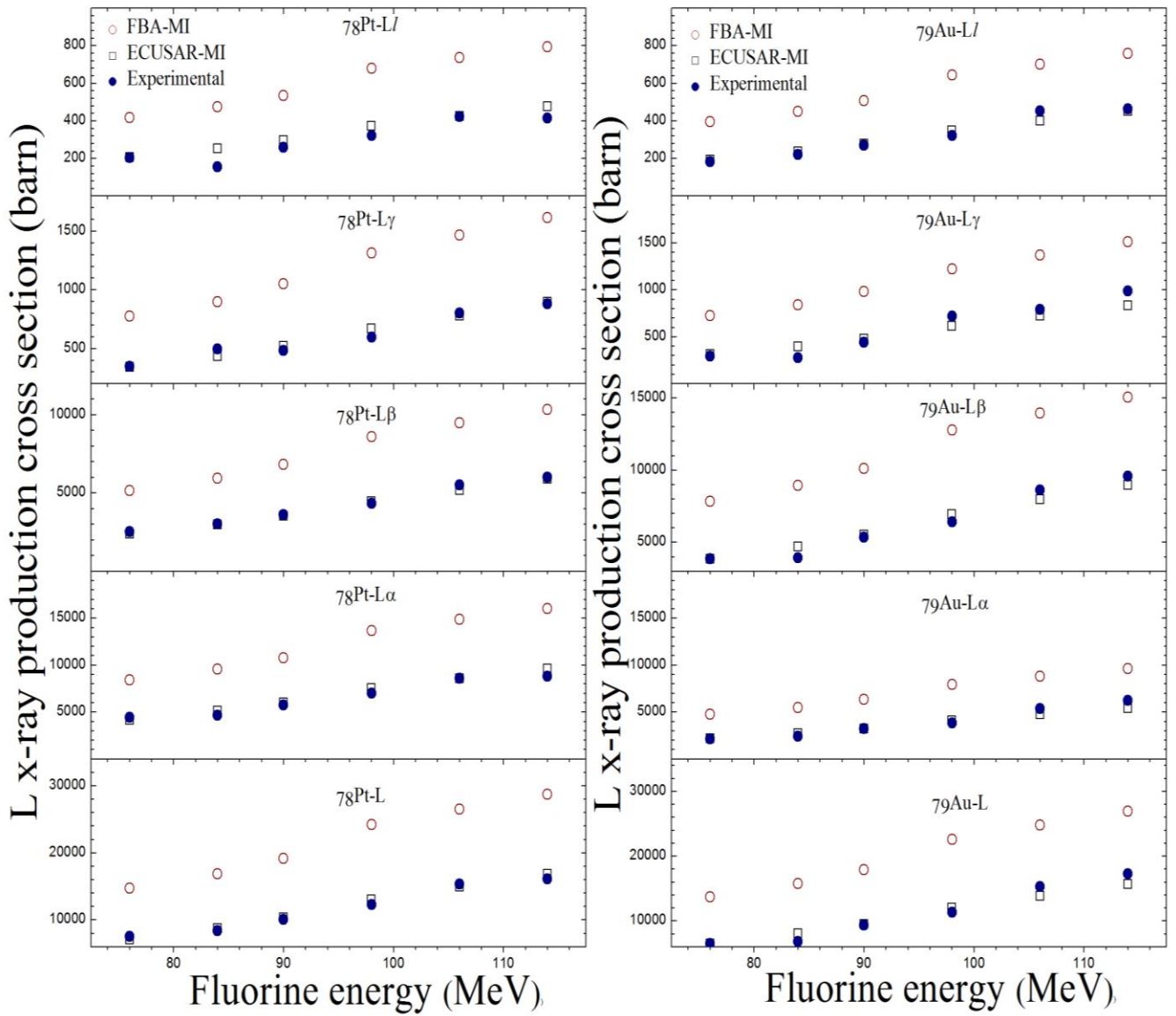


Figure 5

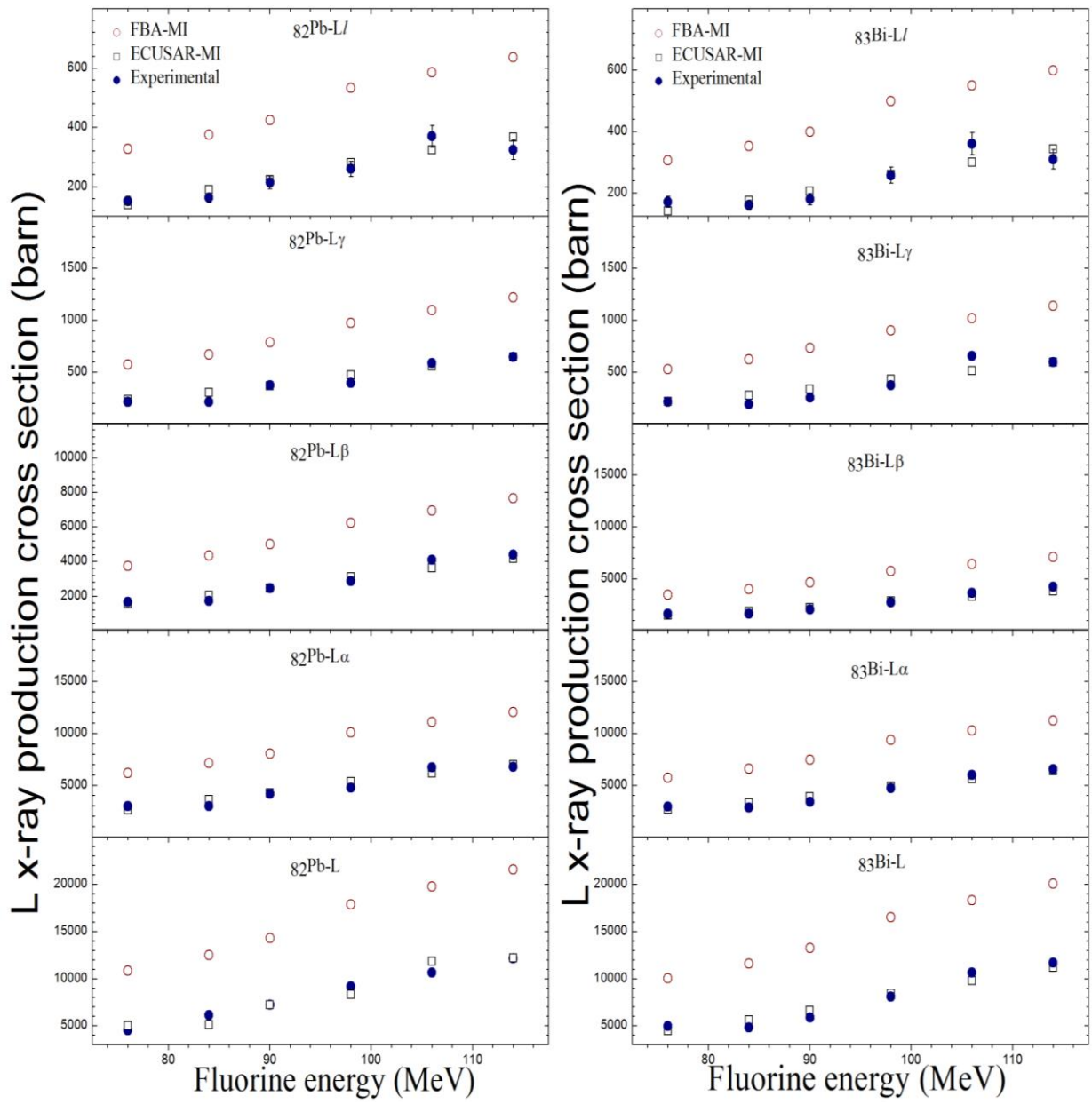


Figure 6

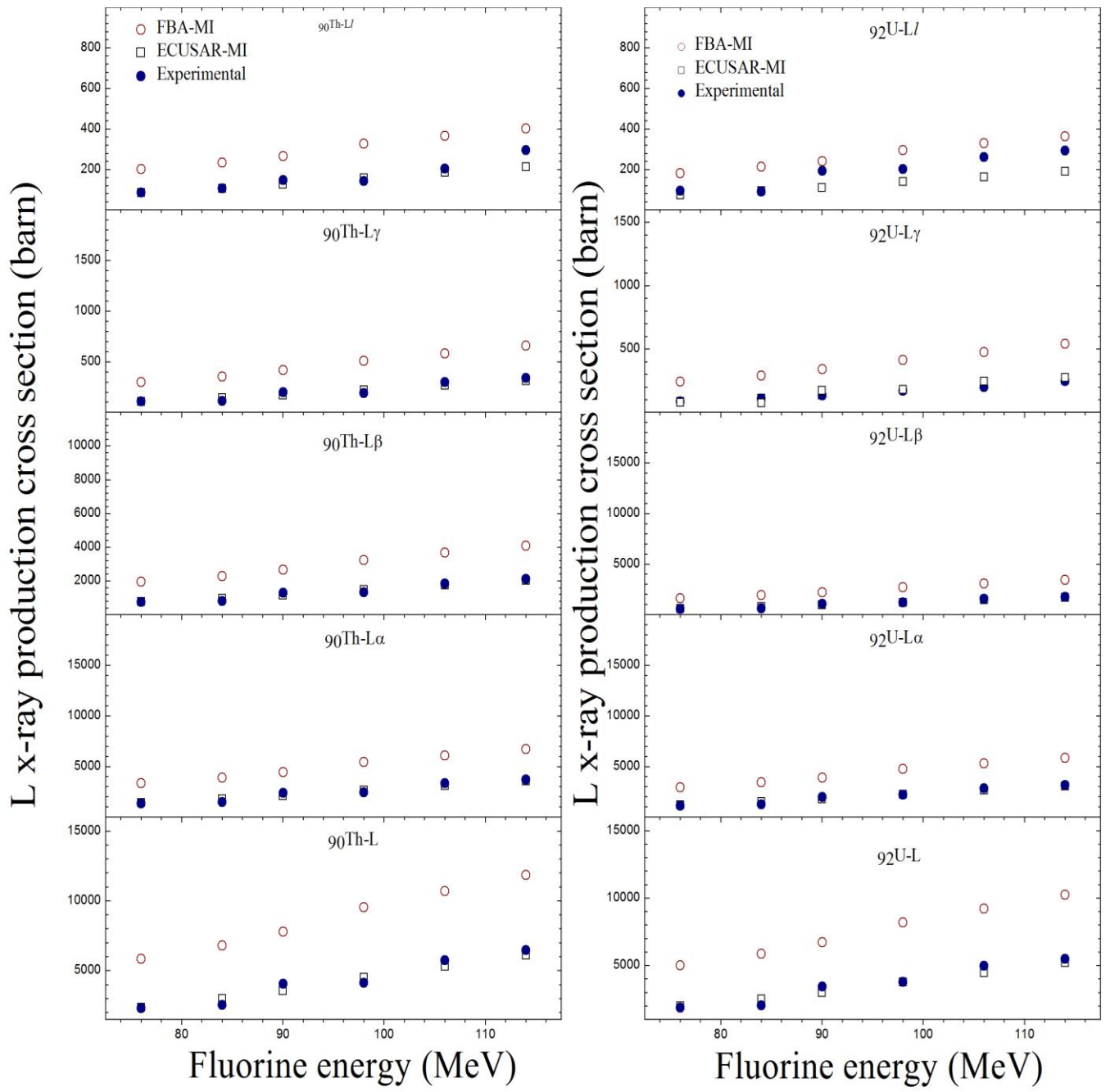


Figure 7